

A modified Ekman layer model

Jaak Heinloo and Aleksander Toompuu

Marine Systems Institute, Tallinn University of Technology, Akadeemia tee 15A, 12618 Tallinn, Estonia; heinloo@phys.sea.ee, alex@phys.sea.ee

Received 26 April 2010, accepted 3 March 2011

Abstract. A modification of the Ekman layer that is able to systematically account for the effects of curvature of the velocity fluctuation streamlines is developed, using the description of turbulent motions. These effects are accounted for through the average vector product of the velocity fluctuations and the local curvature vector of their streamlines at each flow field point. It is shown that this approach enables quantifying the impact of several phenomena (such as the Stokes drift or the incessant generation of vortices with a prevailing orientation of rotation, intrinsic to surface-driven geophysical flows) on the formation of the Ekman layer. The outcome of the suggested modification is compared with the relevant data measured in the Drake Passage.

Key words: Ekman layer, turbulence, modelling.

INTRODUCTION

The Ekman layer velocity data have shown three types of systematic deviations from the situation described by the classical Ekman theory (Ekman 1905). The angle determined between the surface wind stress and the surface drift velocity differs in general from the angle obtained by the classical Ekman solution (Cushman-Roisin 1994). The observed current seems turning less with depth than predicted by the Ekman theory (Weller 1981; Price et al. 1986, 1987; Richman et al. 1987; Wijffels et al. 1994; Chereskin 1995; Schudlich & Price 1998; Chereskin & Price 2001; Lenn & Chereskin 2009), and a large component of shear in the downwind direction near the surface shows no turning (Richman et al. 1987). Attempts have been made to overcome the inconsistency between the recorded data and Ekman theory by using numerical modelling including the depth-varying eddy viscosity (Madsen 1977; Huang 1979) and by complementing the physical background of the Ekman layer description with dynamic processes like the buoyancy flux, Stokes drift, etc. (Coleman et al. 1990; Price & Sundermeyer 1999; Zikanov et al. 2003).

In the current paper the Ekman boundary layer is discussed from the point of view of a modified model based on the turbulence mechanics suggested by Heinloo (2004), called the theory of rotationally anisotropic turbulence (the RAT theory). The RAT theory complements the conventional turbulence mechanics by accounting for the curvature effects of the velocity fluctuation streamlines on the formation of the average flow properties. The complementation allows for a systematic description of the role of some phenomena

intrinsic to the flows with nonzero vorticity in the average flow velocity properties, disregarded within the conventional turbulence mechanics. When applied to the Ekman layer modelling, the curvature effects result in the following. While the classical Ekman model explains the vertical profiles of velocity depending on the wind stress and on one parameter specifying the Ekman depth, the applied RAT theory suggests that the vertical profiles of velocity are formed under the impact of two conditions at the surface (one of which determines the wind stress and the other is interpreted as reflecting the wave conditions) and governed by three parameters with the dimension of length. One parameter describes the effect of the Stokes drift (Phillips 1977) and two other parameters characterize the vertical profile of velocity below the layer influenced by the Stokes drift. It is shown that the modified model embraces the above-discussed deviations of the observed velocity distributions from the classical Ekman solution by one single analytical solution and agrees with data on the Ekman current measured in the Drake Passage (Lenn & Chereskin 2009).

MODEL SETUP

Theoretical background

We start the discussion of the suggested modification of the classical Ekman model with a short description of the theoretical background of the applied RAT theory (Heinloo 2004). The key quantity of this theory is the gyration vector of the turbulent flow field $\mathbf{\Omega}$ (Fig. 1), defined by

$$\mathbf{\Omega} = \langle \mathbf{v}' \times \mathbf{k} \rangle. \quad (1)$$

In Eq. (1) (and henceforth) the angular brackets denote statistical averaging, $\mathbf{v}' = \mathbf{v} - \mathbf{u}$ denotes the fluctuating constituent of the flow velocity, \mathbf{v} is the actual flow velocity, $\mathbf{u} = \langle \mathbf{v} \rangle$ and

$$\mathbf{k} = \frac{\partial \mathbf{e}}{\partial s} \quad (2)$$

is the local curvature vector of the \mathbf{v}' streamline. In Eq. (2) $\mathbf{e} = \mathbf{v}'/v'$ ($v' = |\mathbf{v}'|$) is the unit vector in the direction of \mathbf{v}' and s is the length of the \mathbf{v}' streamline. The norm of the curvature vector \mathbf{k} can be expressed as

$$k = |\mathbf{k}| = \frac{\partial \phi}{\partial s}, \quad (3)$$

where $\partial \phi$ denotes the turn of \mathbf{v}' over the distance ∂s . Using Eqs (2) and (3), we can rewrite Eq. (1) in the form

$$\mathbf{\Omega} = \left\langle \frac{d\phi}{dt} \right\rangle \mathbf{n}, \quad (4)$$

where $\mathbf{n} = \mathbf{e} \times \mathbf{k}/k$ is the unit vector in the direction of $\mathbf{\Omega}$ and $d\phi/dt \equiv v' \partial \phi / \partial s$. From the definition of $\mathbf{\Omega}$ it follows that if there is a prevailing direction of the turn of the velocity fluctuation at a certain location, then $\mathbf{\Omega}$ does not vanish at this location. Introduction of this variable complements the kinematic characterization of the turbulent motion and makes it possible to describe turbulent flow fields in a much more detailed manner compared to classical approaches. Turbulent flows in which $\mathbf{\Omega} \neq 0$ are called rotationally anisotropic.

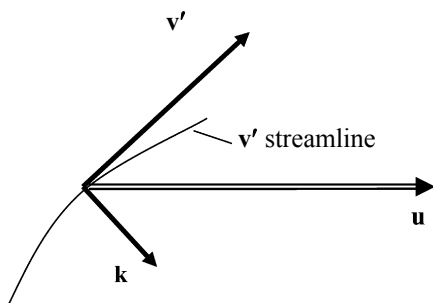


Fig. 1. Representation of the flow field: \mathbf{u} , average velocity; \mathbf{v}' , velocity fluctuation; \mathbf{k} , curvature vector of the velocity fluctuation streamline.

Consider now the dynamical flow characteristic \mathbf{M} corresponding to $\mathbf{\Omega}$, defined as

$$\mathbf{M} = \langle \mathbf{v}' \times \mathbf{R} \rangle, \quad (5)$$

where $\mathbf{R} = \mathbf{k}/k^2$ denotes the local curvature radius-vector of the velocity fluctuation streamline. Substitution of the latter relation into Eq. (5) gives

$$\mathbf{M} = \langle R^2 \mathbf{v}' \times \mathbf{k} \rangle = \left\langle R^2 \frac{d\phi}{dt} \right\rangle, \quad (6)$$

where $R = |\mathbf{R}| = 1/k$. From Eq. (6) it follows that the quantity \mathbf{M} has the meaning of the average angular momentum with $\mathbf{R} = R^2 \mathbf{k}$ in the role of the random moment arm. The defined $\mathbf{\Omega}$ and \mathbf{M} allow us to introduce the effective moment of inertia J as follows:

$$\mathbf{M} = J \mathbf{\Omega}. \quad (7)$$

The quantity \sqrt{J} determines the characteristic spatial scale of the rotationally anisotropic turbulence constituent contributing to $\mathbf{\Omega}$ and \mathbf{M} . It is easy to see that for the turbulent flows with $\mathbf{\Omega} \neq 0$ the turbulence energy (understood here as the energy of velocity fluctuations) $K = \frac{1}{2} \langle v'^2 \rangle$ can be naturally decomposed as follows:

$$K = \frac{1}{2} \mathbf{M} \cdot \mathbf{\Omega} + K^0, \quad (8)$$

where the first term on the right side describes the energy of the rotationally anisotropic part of motion and $K^0 = \frac{1}{2} \langle \mathbf{M}' \cdot \mathbf{\Omega}' \rangle$, where $\mathbf{M}' = \mathbf{v}' \times \mathbf{R} - \mathbf{M}$ and $\mathbf{\Omega}' = \mathbf{v}' \times \mathbf{k} - \mathbf{\Omega}$, is the residual part of the turbulence energy due to the non-orientated fluctuations. Notice that for the non-vanishing \mathbf{M} and/or $\mathbf{\Omega}$, the energy described by the first term on the right side of Eq. (8) does not vanish. Therefore, it is natural to expect that systematically anisotropic local rotation characterized by $\mathbf{\Omega}$ contributes to the dynamical and energetic processes and thus plays a role in forming the average properties of the flow.

The description of turbulent flows with \mathbf{M} , $\mathbf{\Omega} \neq 0$ should be based on the conservation laws of average momentum, angular momentum \mathbf{M} and energy K^0 . The component form of the balance equations expressing the first two of these laws can be expressed as

$$\rho \frac{d}{dt} u_i = \sigma_{ij,j} + \rho f_i, \quad (9)$$

$$\rho \frac{d}{dt} M_i = m_{ij,j} - e_{ijk} \sigma_{jk} + \rho m_i, \quad (10)$$

where $i, j, k = 1, 2, 3$, e_{ijk} is the permutation symbol, ρ is (constant) density of the medium (water), σ_{ij} denotes

the components of the stress tensor, f_i denotes the components of the density of body forces per unit mass, m_{ij} denotes the components of the moment-tensor describing the diffusion of \mathbf{M} , m_i denotes the components of the density of body moments other than described by the first two terms on the right side of Eq. (10) and the index after the comma denotes differentiation along the respective coordinate and Einstein summation is assumed. In essence, Eq. (9) is the averaged Navier–Stokes (Reynolds) equation (with an asymmetric turbulent stress tensor) and Eq. (10) is the averaged equation obtained via the vector multiplication of the equation for \mathbf{v}' (derived from the Navier–Stokes equation) from the right by \mathbf{R} . The technical details of the derivation of Eqs (9) and (10) can be found in Heinloo (2004).

The version of the RAT theory utilized in the current paper particularizes Eqs (9) and (10) by applying the standard closure technique (Heinloo 2004). In particular, the applied closure specifies the vector $\boldsymbol{\sigma}$ with components $e_{ijk}\sigma_{jk}$ in Eq. (10) as

$$\boldsymbol{\sigma} = 4\gamma(\boldsymbol{\Omega} - \boldsymbol{\omega}), \quad (11)$$

in which $\boldsymbol{\omega} = \frac{1}{2}\nabla \times \mathbf{u}$ is the vorticity and γ is called the coefficient of rotational viscosity. The coefficient γ in Eq. (11) couples the $\boldsymbol{\Omega}$ -field to the vorticity field. Note that this coefficient allows for a more detailed description of the flow properties compared to classical approaches where the viscosity is characterized by the turbulent (eddy) viscosity coefficient. Equation (11) suggests that whenever there is vorticity in the field, it results in generation of nonzero $\boldsymbol{\Omega}$ and vice versa.

The model setup

The modification of the classical Ekman model discussed below utilizes Eqs (9) and (10) within the closure introduced in Heinloo (2004). We consider the upper layer of the ocean in the Northern Hemisphere with a constant water density in the right-hand Cartesian coordinate system (x, y, z) , with the coordinate z directed downwards and $z = 0$ at the ocean surface. The ocean is forced by the constant wind stress $\boldsymbol{\tau} = (-\tau, 0, 0)$ directed along the x -axis ($\tau > 0$), and

$$\mathbf{u} = [u_x(z), u_y(z), 0]. \quad (12)$$

For the resulting flow in the coordinate system rotating with the angular velocity, $\boldsymbol{\omega}^0 = (0, 0, -f/2)$, where f is the Coriolis parameter, and for the applied closure, Eqs (9) and (10) can be written as follows:

$$(\mu + \gamma) \frac{\partial^2}{\partial z^2} \mathbf{u} + 2\gamma \nabla \times \boldsymbol{\Omega} + 2\rho \mathbf{u} \times \boldsymbol{\omega}^0 = 0, \quad (13)$$

$$\mathcal{G}J \frac{\partial^2}{\partial z^2} \boldsymbol{\Omega} - 4(\gamma + \kappa) \boldsymbol{\Omega} + 2\gamma \nabla \times \mathbf{u} = 0. \quad (14)$$

Equations (13) and (14) differ from the respective equations derived in Heinloo (2004) by the presence of the Coriolis term in Eq. (13). Here (in addition to J and γ explained above) μ is the coefficient of turbulent shear viscosity quantifying the transfer of energy from the average flow to the energy of the non-orientated turbulence constituent K^0 , κ is the coefficient quantifying the energy transfer from $\frac{1}{2}\mathbf{M} \cdot \boldsymbol{\Omega}$ to K^0 and \mathcal{G} is the coefficient of diffusion of the angular momentum \mathbf{M} . It follows from Eqs (13) and (14) that only the horizontal components of $\boldsymbol{\Omega}$ are coupled to the flow velocity, therefore, similar to the flow velocity (Eq. (12)), we shall assume that $\boldsymbol{\Omega} = [\Omega_x(z), \Omega_y(z), 0]$. For $\gamma = 0$ Eq. (13) reduces to the equation of the classical Ekman model and Eq. (14) to an additional equation interpreted as describing the effect of the Stokes drift. In what follows we assume that $\gamma \neq 0$, consequently, the effect of the Stokes drift is coupled with the motions described by the classical Ekman model.

The solution of Eqs (13) and (14) is assumed to satisfy the following boundary conditions:

$$\lim_{z \rightarrow \infty} \mathbf{u}, \boldsymbol{\Omega} = 0, \quad (15)$$

$$(\mu + \gamma) \left. \frac{\partial \mathbf{u}}{\partial z} \right|_{z=0} + 2\gamma \mathbf{E} \cdot \boldsymbol{\Omega}(0) = \boldsymbol{\tau}, \boldsymbol{\Omega}(0) = c\boldsymbol{\omega}(0). \quad (16)$$

In Eqs (16) \mathbf{E} is the Levi-Civita tensor with components e_{ijk} , $\boldsymbol{\omega} = \frac{1}{2}\nabla \times \mathbf{u}$ is the vorticity and c is a constant, $0 < c < 1$. The second condition in Eqs (16) simply means that $\boldsymbol{\Omega}$ and $\boldsymbol{\omega}$ are collinear at the boundary $z = 0$. Consequently, the first condition in Eqs (16) can be rewritten as

$$\mu_s \left. \frac{\partial \mathbf{u}}{\partial z} \right|_{z=0} = -\boldsymbol{\tau}, \quad (17)$$

where $\mu_s = \mu + \gamma(1 - c) \geq \mu$. All flow-specific coefficients as well as J in Eqs (13) and (14) are treated as constants.

DISCUSSION

Solution for the flow velocity

Defining $\tilde{u} = u_x + iu_y$ and $\tilde{\Omega} = \Omega_x + i\Omega_y$, where i is the imaginary unit, from Eqs (13)–(17) we have

$$(\mu + \gamma) \frac{\partial^2 \tilde{u}}{\partial z^2} + 2\gamma i \frac{\partial \tilde{\Omega}}{\partial z} + i\rho f \tilde{u} = 0, \quad (18)$$

$$gJ \frac{\partial^2 \tilde{\Omega}}{\partial z^2} - 4(\gamma + \kappa) \tilde{\Omega} + 2i\gamma \frac{\partial \tilde{u}}{\partial z} = 0, \quad (19)$$

$$\lim_{z \rightarrow \infty} \tilde{u}, \tilde{\Omega} = 0, \quad \left. \frac{\partial \tilde{u}}{\partial z} \right|_{z=0} = -\frac{\tau}{\mu_s} \quad \text{and} \quad \tilde{\Omega}(0) = i \frac{c}{2} \left. \frac{\partial \tilde{u}}{\partial z} \right|_{z=0}. \quad (20)$$

The solution of Eqs (18)–(20) for \tilde{u} is expressed as

$$\tilde{u} = \tilde{u}_1(z) + \tilde{u}_2(z), \quad (21)$$

where

$$\tilde{u}_1 = \tilde{u}_1(0) \exp(\lambda_1 z) \quad \text{and} \quad \tilde{u}_2 = \tilde{u}_2(0) \exp(\lambda_2 z). \quad (22)$$

In Eq. (22), λ_1 and λ_2 are the roots of the biquadratic equation

$$\lambda^4 - \left[\frac{1}{\ell^2} - \frac{i}{\ell_1^2} \right] \lambda^2 - \frac{1}{\ell^2} \frac{i}{\ell_2^2} = 0, \quad (23)$$

in which

$$\frac{1}{\ell^2} = 4 \frac{1}{J} \frac{\mu_{\text{ef}}(\gamma + \kappa)}{g(\mu + \gamma)}, \quad \frac{1}{\ell_1^2} = \frac{\rho f}{\mu + \gamma} < \frac{1}{\ell_2^2} = \frac{\rho f}{\mu_{\text{ef}}}, \quad (24)$$

and $\mu_{\text{ef}} = \mu + \gamma \kappa (\gamma + \kappa)^{-1}$. Only the values of λ_1 and λ_2 with negative real parts are compatible with the boundary conditions stated in Eq. (15) and are applied hereafter. The velocity constituents $\tilde{u}_1(0)$ and $\tilde{u}_2(0)$ are specified as

$$\tilde{u}_1(0) = \frac{\tau}{\mu_s} \frac{-\lambda_1 + B\lambda_2 \exp(i\pi/4)}{\lambda_1^2 - \lambda_2^2} \quad (25)$$

and

$$\tilde{u}_2(0) = \frac{\tau}{\mu_s} \frac{\lambda_2 - B\lambda_1 \exp(i\pi/4)}{\lambda_1^2 - \lambda_2^2}, \quad (26)$$

where $B = \mu_s \ell_2 (\mu_{\text{ef}} \ell)^{-1} > 0$.

Equations (21)–(26) represent the vertical distribution of the average flow velocity depending on $\tau \mu_s^{-1}$, $\mu_s \mu_{\text{ef}}^{-1}$ and on three characteristics of turbulence properties of the medium $\ell < \ell_2 < \ell_1$ with the dimension of length.

Properties of the vertical structure of velocity

Consider the solution of Eq. (23) for λ_1^2 and λ_2^2 in the following representation:

$$\lambda_1^2 = |\lambda_1^2| \exp(i\psi) \quad \text{and} \quad \lambda_2^2 = |\lambda_2^2| \exp[i(3\pi/2 - \psi)], \quad (27)$$

where $0 \leq \psi \leq \pi/2$, $|\lambda_1^2| = |\lambda_1|^2$ and $|\lambda_2^2| = |\lambda_2|^2$, while $|\lambda_1| |\lambda_2| = (\ell \ell_2)^{-1}$ and $|\lambda_1| > |\lambda_2|$. Using Eq. (27), we have for λ_1 and λ_2

$$\lambda_1 = -|\lambda_1| \exp(i\varphi)$$

and

$$\lambda_2 = |\lambda_2| \exp[i(3\pi/4 - \varphi)] = -|\lambda_2| \exp[-i(\varphi + \pi/4)],$$

where $0 \leq \varphi = \psi/2 \leq \pi/4$. When denoting the e -folding scales for \tilde{u}_1 and \tilde{u}_2 by

$$h_{11} = -\frac{1}{\text{Re } \lambda_1} = \frac{1}{|\lambda_1| \cos \varphi} > 0$$

and

$$h_{21} = -\frac{1}{\text{Re } \lambda_2} = \frac{1}{|\lambda_2| \cos(\varphi + \pi/4)} > 0,$$

and the respective rotation scales of \tilde{u}_1 and \tilde{u}_2 by

$$h_{12} = -\frac{1}{\text{Im } \lambda_1} = \frac{1}{|\lambda_1| \sin \varphi} > 0$$

and

$$h_{22} = \frac{1}{\text{Im } \lambda_2} = \frac{1}{|\lambda_2| \sin(\varphi + \pi/4)} > 0,$$

the expressions for \tilde{u}_1 and \tilde{u}_2 in Eq. (22) can also be rewritten as

$$\begin{aligned} \tilde{u}_1 &= \tilde{u}_1(0) \exp\left(-\frac{z}{h_{11}}\right) \exp\left(-i \frac{z}{h_{12}}\right), \\ \tilde{u}_2 &= \tilde{u}_2(0) \exp\left(-\frac{z}{h_{21}}\right) \exp\left(i \frac{z}{h_{22}}\right). \end{aligned} \quad (28)$$

In the following we interpret the velocity constituents \tilde{u}_1 and \tilde{u}_2 as the Stokes drift and the Ekman drift velocity constituents, respectively.

Let us emphasize the following properties of the solution given by Eqs (21) and (28).

1. For $\gamma = c = 0$ and $\ell \ll \ell_E = (2\mu)^{1/2}(\rho f)^{-1/2}$, where ℓ_E is the Ekman depth in its classical sense, we have $\lambda_1 = -\ell^{-1}$, $\lambda_2 = (i-1)\ell_E^{-1}$, $\tilde{u}_1(0) = 0$, $\tilde{u}_2(0) = \tau(\rho f \mu)^{-1/2} \exp(i\pi/4)$, $h_{21} = h_{22} = \ell_E$ and the solution given by Eqs (21) and (28) reduces to the classical solution for the Ekman boundary layer

$$\tilde{u} = \frac{\tau}{\sqrt{\rho f \mu}} \exp\left(-\frac{z}{\ell_E}\right) \exp\left[i\left(\frac{z}{\ell_E} + \frac{\pi}{4}\right)\right]. \quad (29)$$

2. The integral volume transport in the Ekman layer,

$$\int_0^{\infty} \tilde{u} dz = \frac{i\tau}{\rho f},$$

coincides with the transport following from the classical Ekman's theory.

3. Due to

$$\tilde{u}(0) = \tilde{u}_1(0) + \tilde{u}_2(0) = -\frac{\tau}{\mu_s} \frac{1 + B \exp(i\pi/4)}{\lambda_1 + \lambda_2},$$

the angle between the surface wind stress and the surface drift velocity in general differs from $\pi/4$ predicted by the classical Ekman solution. In particular, for $\ell \ll \ell_E$ (considered as the most typical) we have $\tilde{u}(0) \approx -\tau\ell/\mu_s(1 + B \exp(i\pi/4))$ determining the angle between the surface wind stress and surface drift velocity between 0 (the Stokes drift situation) and $\pi/4$ (the classical Ekman situation).

4. The e -folding scale of \tilde{u}_2 exceeds the e -folding scale of \tilde{u}_1 ($h_{21} > h_{11}$), i.e., the characteristic vertical extent of the Ekman drift layer is larger than the characteristic vertical extent of the Stokes drift layer.
5. Due to the opposite signs of the arguments of the exponent $-iz/h_{12}$ and iz/h_{22} in Eq. (28), the velocity constituents \tilde{u}_1 (the Stokes drift velocity constituent) and \tilde{u}_2 (the Ekman drift velocity constituent) rotate with depth in opposite directions.
6. While the e -folding scale of the Ekman drift velocity constituent \tilde{u}_2 exceeds its rotation depth scale ($h_{21} > h_{22}$), the rotation scale of the Stokes drift velocity constituent \tilde{u}_1 exceeds its e -folding scale ($h_{11} < h_{12}$).
7. While the scales h_{21} and h_{11} both decrease, h_{22} and h_{12} increase for decreasing φ (so that for $\varphi = 0$ we have $h_{12} = h_{22}$). Therefore, the properties of the Ekman and Stokes layers are in general interdependent.

Although the discussed solution was derived for the Northern Hemisphere, it holds also for the Southern Hemisphere (where the y -axis is reversed to form the left-hand coordinate system (x, y, z)).

Comparison with the observed data

Properties 1–7 demonstrate that the derived solution is sufficiently flexible to mimic the observed velocity distributions (cited in the Introduction) that diverge from the vertical structure predicted by the classical Ekman solution. In agreement with Cushman-Roisin (1994), the modification includes the situation with the angle between the wind and the surface drift velocity vectors different from $\pi/4$. Figure 2 exemplifies this situation on the velocity spiral of the non-dimensional velocity $\mu_s(\tau\ell)^{-1}\tilde{u}$ calculated for $\mu_s\mu_{ef}^{-1} = 0.07$, $\ell = 10$ m, $\ell_1 = 60$ m and $\ell_2 = 50$ m. The surface velocity is veering by 18.3° to the right of the wind direction. On the basis of the observed data it has been stated in several investigations (Weller 1981; Price et al. 1986, 1987; Wijffels et al. 1994; Chereskin 1995; Schudlich & Price 1998; Price & Sundermeyer 1999; Chereskin & Price 2001; Lenn & Chereskin 2009) that the rotation scale of velocity profiles exceeds the e -folding scale of the velocity norm. The suggested

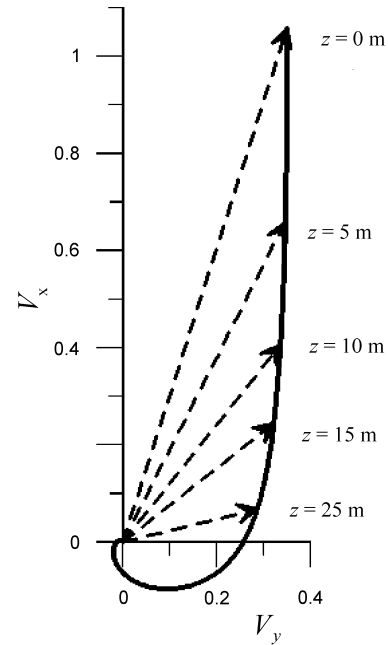


Fig. 2. Velocity spiral for the modelled non-dimensional velocity $\mu_s(\tau\ell)^{-1}\tilde{u}$, corresponding to $\mu_s\mu_{ef}^{-1} = 0.07$, $\ell = 10$ m, $\ell_1 = 60$ m and $\ell_2 = 50$ m ($V_x = \mu_s(\tau\ell)^{-1}\text{Re}\tilde{u}$ and $V_y = \mu_s(\tau\ell)^{-1}\text{Im}\tilde{u}$). The velocity modulus decreases e times at a depth of 15 m and the velocity vector turns by 1 rad at a depth of 24 m relative to their values at the surface.

modified solution includes this effect. As an example, in case of the velocity spiral shown in Fig. 2, the e -folding and the rotation scales of the velocity are 15 and 24 m, respectively.

Figure 3 presents the data of the flow velocity relative to the reference level at $z = 98$ m (circles) collected in the Drake Passage (adopted from Lenn & Chereskin 2009) together with the corresponding velocity distributions calculated from Eqs (21) and (28) (solid curves) and the Ekman solution calculated from Eq. (29) (dashed curves). The modelled velocity distribution is calculated for $\mu_s \mu_{ef}^{-1} = 0.77$, $\ell = 14$ m, $\ell_1 = 32$ m, $\ell_2 = 31$ m, $\tau \mu_s^{-1} = 0.115$ s $^{-1}$ and the Ekman velocity distribution for $\ell_E = 44$ m, $\tau(\rho f \mu)^{-1/2} = 0.032$ m s $^{-1}$. It can be seen in Fig. 3 that, firstly, the modified solution fits better the observed data than the Ekman solution. Secondly, the e -folding scale of the Ekman layer (ℓ_E) predicted by the Ekman solution exceeds the characteristic e -folding scale ($\max\{\ell_1, \ell_2\}$) predicted by the modified solution. Thirdly, the classical Ekman solution matches the observed data in Fig. 3 rather well, therefore the rotation scale of the vertical distribution of velocity is close to its e -folding scale. This conclusion, however, contradicts Lenn & Chereskin (2009), where, based on the same data set, the rotation scale of the vertical distribution of velocity has been estimated to exceed its e -folding scale by 2–3 times. The indicated contradiction follows from a specific feature of Lenn & Chereskin (2009) analysis. Their analysis was applied to

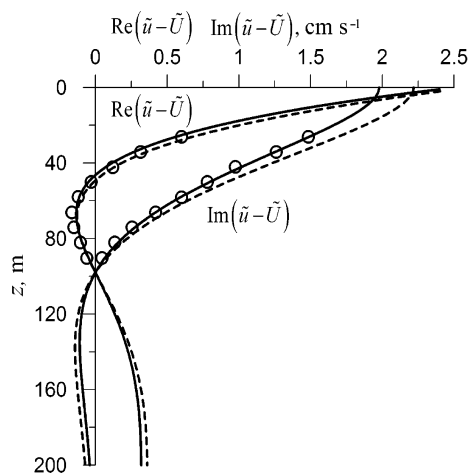


Fig. 3. The depth-dependence of the velocity components $\text{Re}(\tilde{u} - \tilde{U})$ and $\text{Im}(\tilde{u} - \tilde{U})$, where \tilde{U} is the velocity at the reference level $z = 98$ m, calculated according to the suggested model for $\mu_s \mu_{ef}^{-1} = 0.77$, $\ell = 14$ m, $\ell_1 = 32$ m, $\ell_2 = 31$ m, $\tau \mu_s^{-1} = 0.115$ s $^{-1}$ (solid curves) and according to the Ekman model for $\ell_E = 44$ m, $\tau(\rho f \mu)^{-1/2} = 0.032$ m s $^{-1}$ (dashed curves) compared with data (circles) adopted from Lenn & Chereskin (2009).

the velocity data from which the velocity at the assumed reference level of $z = 98$ m had been subtracted. The resulting velocity equals to zero at the selected reference level. As a consequence, the e -folding scale becomes dependent on the reference level depth and no more characterizes the underlying physical process.

CONCLUSIONS

The Ekman layer studies (Huang 1979; Davis et al. 1981; Weller 1981; Price et al. 1986, 1987; Richman et al. 1987; Weller et al. 1991; Cushman-Roisin 1994; Wijffels et al. 1994; Chereskin 1995; Schudlich & Price 1998; Price & Sundermeyer 1999; Chereskin & Price 2001; Lenn & Chereskin 2009) have shown that the observed vertical distributions of velocity in the ocean Ekman layer often deviate from the distribution predicted by the Ekman theory. The suggested modified Ekman model explains the observed deviations from the point of view of the turbulence mechanics in Heinloo (2004) accounting for the curvature effects of the velocity fluctuation streamlines on the formation of the average flow properties. The curvature effects are accounted for through the average vector product of the velocity fluctuations and the local curvature vectors of their streamlines at all points of the flow field. This approach makes it possible to systematically account for phenomena (such as the Stokes drift or the generation of rotationally anisotropic part of the motion) affecting the structure of the Ekman layer. It is shown that the additional included effects can explain the observed deviations from the Ekman theory and agree with the data measured in the Drake Passage adopted from Lenn & Chereskin (2009).

Acknowledgements. The authors thank the anonymous referee whose critical comments helped to modify the style of the paper and to bring the presentation to the commonly accepted standards.

REFERENCES

- Chereskin, T. K. 1995. Direct evidence for an Ekman balance in the California Current. *Journal of Geophysical Research*, **100**, 18261–18269.
- Chereskin, T. K. & Price, J. F. 2001. Ekman transport and pumping. In *Encyclopedia of Ocean Sciences* (Steele, J., Thorpe, S. & Turekian, K., eds), pp. 809–815. Academic Press.
- Coleman, G. N., Ferziger, J. H. & Spalart, P. R. 1990. A numerical study of the turbulent Ekman layer. *Journal of Fluid Mechanics*, **213**, 313–348.
- Cushman-Roisin, B. 1994. *Introduction to Geophysical Fluid Dynamics*. Prentice Hall, 320 pp.

- Davis, R., deSzoeke, R., Halpern, D. & Niiler, P. 1981. Variability in the upper ocean during MILE. Part 1: The heat and momentum balances. *Deep-Sea Research*, **28A**, 1427–1451.
- Ekman, V. W. 1905. On the influence of the Earth's rotation on ocean currents. *Arkiv för Matematik, Astronomi och Fysik*, **2**, 1–53.
- Heinloo, J. 2004. The formulation of turbulence mechanics. *Physics Review E*, **69**, 056317.
- Huang, N. E. 1979. On surface drift currents in the ocean. *Journal of Fluid Mechanics*, **91**, 191–208.
- Lenn, Y.-D. & Chereskin, T. K. 2009. Observations of Ekman currents in the Southern Ocean. *Journal of Physical Oceanography*, **39**, 768–779.
- Madsen, O. S. 1977. A realistic model of the wind-induced Ekman boundary layer. *Journal of Physical Oceanography*, **7**, 248–255.
- Phillips, O. M. 1977. *Dynamics of the Upper Ocean*. Cambridge University Press, 336 pp.
- Price, J. F. & Sundermeyer, M. A. 1999. Stratified Ekman layers. *Journal of Geophysical Research*, **104**(C9), 20467–20494.
- Price, J. F., Weller, R. A. & Pinkel, R. 1986. Diurnal cycling: observations and models of the upper ocean response to diurnal heating, cooling, and wind mixing. *Journal of Geophysical Research*, **91**, 8411–8427.
- Price, J. F., Weller, R. A. & Schudlich, R. R. 1987. Wind-driven ocean currents and Ekman transport. *Science*, **238**, 1534–1538.
- Richman, J. G., deSzoeke, R. A. & Davis, R. E. 1987. Measurements of near-surface shear in the ocean. *Journal of Geophysical Research*, **92**, 2851–2858.
- Schudlich, R. R. & Price, J. F. 1998. Observations of seasonal variation in the Ekman layer. *Journal of Physical Oceanography*, **28**, 1187–1204.
- Weller, R. A. 1981. Observations of the velocity response to wind forcing in the upper ocean. *Journal of Geophysical Research*, **86**, 1969–1977.
- Weller, R. A., Rudnick, D. L., Eriksen, C. C., Polzin, K. L., Oakey, N. S., Toole, J. W., Schmitt, R. W. & Pollard, R. T. 1991. Forced ocean response during the Frontal Air–Sea Interaction Experiment. *Journal of Geophysical Research*, **96**, 8611–8638.
- Wijffels, S., Firing, E. & Bryden, H. L. 1994. Direct observations of the Ekman balance at 10° N in the Pacific. *Journal of Physical Oceanography*, **24**, 1666–1679.
- Zikanov, O., Slinn, D. N. & Dhanak, M. R. 2003. Large-eddy simulations of the wind-induced turbulent Ekman layer. *Journal of Fluid Mechanics*, **495**, 343–368.

Modifitseeritud Ekmani kihi mudel

Jaak Heinloo ja Aleksander Toompuu

On esitatud modifitseeritud klassikaline Ekmani kihi mudel. See arvestab kiiruse pulsatsiooni voolujoonte kõverusest tulenevat mõju keskmise kiiruse väljale ja selle väljundiks on analüütiline kiiruse vertikaalse jaotuse valem. On näidatud, et tuletatud valem kirjeldab olukordi, kus tuule kiiruse ja pinnahoovuse kiiruse vektorite vaheline nurk erineb nurgast, mis tuleneb klassikalisest Ekmani lahendist, ning kus kiiruse e -kordse kahanemise sügavuse mastaap erineb kiirusvektori pöörlemis sügavuse mastaabist. Mudelist tulenevat kiiruse vertikaalset jaotust on võrreldud Drake'i väinas mõõdetud kiiruse andmetega, mis on avaldatud Lenni ja Chereskini poolt 2009. aastal.